J Therm Anal Calorim (2012) 107:1093–1103
DOI 10.1007/s10973-011-1797-x

Non-isothermal oxidation kinetics of single- and multi-walled carbon nanotubes up to 1273 K in ambient

Soumya Sarkar · Probal Kr. Das

Received: 30 March 2011 / Accepted: 8 July 2011 / Published online: 27 July 2011

Abstract Non-isothermal oxidation kinetics of single- and multi-walled carbon nanotubes (CNTs) have been studied using thermogravimetry up to 1273 K in ambient using multiple heating rates. One single heating rate based model-fitting technique and four multiple heating rates based model-free isoconversional methods were used for this purpose. Depending on nanotube structure and impurity content, average activation energy (E_a), pre-exponential factor (A), reaction order (n), and degradation mechanism changed considerably. For multi-walled CNTs, E_a and A evaluated using model-fitting technique were ranged from 142.31 to 178.19 kJ mol^{-1}, respectively, and from 1.71×10^5 to 5.81×10^7 s^{-1}, respectively, whereas, E_a for single-walled CNTs ranged from 83.84 to 148.68 kJ mol^{-1} and A from 2.55×10^2 to 1.18×10^7 s^{-1}. Although, irrespective of CNT type, the model-fitting method resulted in a single kinetic triplet i.e., E_a, A, and reaction mechanism, model-free isoconversional methods suggested that thermal oxidation of these nanotubes could be either a simple single-step mechanism with almost constant activation energy throughout the reaction span or a complex process involving multiple mechanisms that offered varying E_a with extent of conversion. Criado method was employed to predict degradation mechanism(s) of these CNTs.

Keywords Carbon nanotube · TG · Non-isothermal kinetics · Model-fitting · Isoconversional · Electron microscopy

S. Sarkar · P. Kr. Das (✉)
Non-oxide Ceramic and Composite Division, Central Glass and Ceramic Research Institute (CSIR), Kolkata 700032, India
e-mail: probal@cgcri.res.in

Introduction

Having exceptional blending of essential material properties, CNT either single-walled (SWNT) or multi-walled (MWNT) is presently considered to be the most promising candidate for next generation nanotechnology [1]. As individual or combined with other suitable materials, CNTs have already proved potential use in diverse field including structural, transportation, medicine, electronics, and energy [1–4]. In many of such applications, components have to withstand various temperatures and thermal cycling in different environments [5, 6] and consequently, a fair knowledge on thermal stability and oxidation kinetics of various CNTs for real life applications is very important. However, limited reports are available in literature that dealt with oxidation patterns of CNTs and reported activation energy for SWNTs lie between 120 and 140 kJ mol^{-1} and that for MWNTs lie between 150 and 290 kJ mol^{-1} [7–11]. In a recent communication, Sarkar et al. [11] also reported that thermal degradation of MWNT should follow a first order reaction kinetics in its as-received form whereas after high temperature treatment in inert atmosphere, thermal stability of MWNTs increased significantly and followed higher order reaction kinetics. Therefore, it is equally important to realize the effect of structural features of carbon nanotubes (CNTs) e.g., purity and type of CNT used, diameter and length of CNTs, defect types and concentration, catalyst type and content on their thermal stability. Although, kinetic studies of thermal degradation using various model-fitting and model-free methods are available [11–20], inconsistencies among results obtained from these two methodologies have also been reported [21–29]. The international congress on thermal analysis and calorimetry (ICTAC) dealt meticulously on computational aspects of studying kinetics of

thermal degradation using model-fitting as well as model-free techniques [21, 22]. The research group strongly emphasized on the fact that kinetics of thermal degradation of a solid are most often multi-step reaction process and should not be described by a single kinetic triplet and therefore, single heating rate based model-fitting methods should be avoided where a single kinetic triplet is turned out to adequately describe the complete reaction mechanism of thermal degradation path disregarding its complexity [22]. On the other hand, multiple heating rate based model-free methods which are inherently free from errors connected with the choice of a model can be suitably used to investigate the complexity of a degradation process where occurrence of different reaction mechanism leads to the change in effective (or local) activation energy ($E_{a,\alpha}$) with extent of conversion (isoconversional method) [12–14, 24–29] and temperature (non-parametric kinetics method) [30, 31]. Further, *Arrhenius* parameters evaluated using model-free techniques facilitate modeling of a degradation process in other temperature spans than those applied in the measurement. However, the experimental part of ICTAC project primarily used calcium carbonate and ammonium perchlorate and their isothermal or non-isothermal degradation kinetics either in vacuum or in nitrogen atmosphere and also suggested to verify such inconsistency and/or incapability of model-fitting methods for performing kinetic analysis of other materials [22]. Considering the above fact, in this report, both single heating rate based model-fitting Coats-Redfern (CR) technique and multiple heating rate based model-free isoconversional Friedman (FR), Kissinger–Akahira–Sunose (K-A-S), Tang (T), and Flynn–Wall–Ozawa (F–W–O) techniques were employed for analyzing the kinetics of thermal degradation of commercially available SWNTs and MWNTs under non-isothermal condition in ambient air up to 1273 K at three experimental heating rates. The purpose was to assess the extent of deviation (if any) between model-fitting and model-free techniques in kinetic analysis of thermal degradation of the most promising candidate in the field of nanoscience and technology i.e., CNT as well as to analyze influence of structural features of nanotubes on non-isothermal degradation. Further, thermal oxidative degradation mechanism(s) of present CNT specimens were predicted using Criado method [32]. Transmission electron microscopic (TEM) analysis of each CNT specimen was carried out to reveal the structural features.

Theoretical background of kinetic analysis

Kinetic parameters of thermal degradation of a material can be evaluated using degree of conversion or conversion factor i.e., α which is expressed as [11, 12]:

$$\alpha = (m_i - m_t)/(m_i - m_f) \tag{1}$$

where m_i, m_t, and m_f are initial, instantaneous, and final mass of sample, respectively. Now, for non-isothermal degradation, the kinetic equation is [11, 12]:

$$\frac{d\alpha}{dt} = \beta\frac{d\alpha}{dT} = k(T)f(\alpha), \tag{2}$$

where $d\alpha/dt$ = degradation rate; $\beta = dT/dt$ = experimental heating rate; $f(\alpha)$ = conversion function; T is absolute temperature in Kelvin and $k(T)$ = rate constant which is described by the well-known *Arrhenius* expression as [11, 12]:

$$k(T) = A\exp\left(-\frac{E_a}{RT}\right), \tag{3}$$

where R is the universal gas constant (8.314 J mol^{-1} K^{-1}). From Eqs. 3 and 2 one obtains:

$$\frac{d\alpha}{dt} = \beta\frac{d\alpha}{dT} = Af(\alpha)\exp\left(-\frac{E_a}{RT}\right). \tag{4}$$

Equation 4 is treated as the differential form of non-isothermal rate law. To obtain integral form of rate law Eq. 4 needs to be integrated with respect to "T" i.e., [13, 18]:

$$\int_0^\alpha \frac{d\alpha}{f(\alpha)} = \int_0^\alpha \frac{d\alpha}{(1-\alpha)^n} = g(\alpha) = \frac{A}{\beta}\int_0^T \exp\left(-\frac{E_a}{RT}\right)dT, \tag{5}$$

where $f(\alpha) = (1-\alpha)^n$; n is the order of reaction; $g(\alpha)$ is integral conversion function that depends on $f(\alpha)$ and expressed as [18]:

$$g(\alpha) = -\ln(1-\alpha) \quad \text{for } n = 1 \tag{6a}$$

and

$$g(\alpha) = \frac{(1-\alpha)^{(1-n)} - 1}{(n-1)} \quad \text{for } n \neq 1. \tag{6b}$$

Now, assuming $x = E_a/RT$, R.H.S of Eq. 5 can be written as [13, 18]:

$$\frac{A}{\beta}\int_0^T \exp\left(-\frac{E_a}{RT}\right)dT = \frac{AE_a}{\beta R}\int_0^x \frac{\exp(-x)}{x^2}dx = \frac{AE_a}{\beta R}p(x), \tag{7}$$

where $p(x)$ is the exponential integral which has no analytical solution but many mathematical approximations.

Model-fitting method

CR method [11, 12, 15–20, 24, 28, 29, 33]

The thermogravimetry (TG) data of all four CNT specimens were first treated with the most popular single heating

rate based model-fitting technique proposed by CR to calculate the best feasible kinetic triplet of thermal oxidation of present CNTs. The integral CR method utilizes the asymptotic series expansion in approximating $p(x)$ of Eq. 5 as:

$$p(x) \cong \frac{\exp(-x)}{x^2}. \tag{8}$$

Therefore, from Eqs. 5, 7, and 8 we get:

$$g(\alpha) = \frac{ART^2}{\beta E_a}\exp\left(-\frac{E_a}{RT}\right)[\because x = E_a/RT]. \tag{9}$$

So, from Eqs. 6a, 6b, and 9 the CR expressions finally take the following forms:

$$\text{For } n = 1; \quad \ln\left(-\frac{\ln(1-\alpha)}{T^2}\right) = \ln\left(\frac{AR}{\beta E_a}\right) - \frac{E_a}{RT} \tag{10a}$$

$$\text{For } n \neq 1; \quad \ln\left(\frac{(1-\alpha)^{(1-n)}-1}{T^2(n-1)}\right) = \ln\left(\frac{AR}{\beta E_a}\right) - \frac{E_a}{RT}. \tag{10b}$$

Depending on the order of reaction, a plot of L.H.S of either Eq. 10a or 10b versus $1/T$ should be straight line whose slope and intercept gives E_a and A.

Isoconversional methods

FR method [28]

The differential isoconversional method proposed by FR is based on Eq. 4 in logarithmic form and expressed as:

$$\ln\left[\beta\left(\frac{d\alpha}{dT}\right)_\alpha\right] = \ln\left(A_\alpha f(\alpha)_\alpha\right) - \frac{E_{a,\alpha}}{RT_\alpha}. \tag{11}$$

At constant α, plot of L.H.S. versus $1/T_\alpha$ of Eq. 11 should be straight line whose slope is used to evaluate the local activation energy ($E_{a,\alpha}$).

K–A–S method [12–15, 24–26, 28, 29]

The K–A–S method is one of the best integral isoconversional methods formulated based on CR approximation of $p(x)$ for $20 < x < 50$ and expressed as:

$$\ln\left(\frac{\beta}{T^2}\right) = \ln\left(\frac{AR}{g(\alpha) * E_{a,\alpha}}\right) - \left(\frac{E_{a,\alpha}}{RT}\right). \tag{12}$$

According to Eq. 12, for constant α, plot of $\ln(\beta/T^2)$ versus $(1/T)$ obtained from curves recorded at three heating rates, should be straight line whose slope can be used to calculate the $E_{a,\alpha}$.

T method [28, 34]

Tang et al. [34] has proposed a new precise approximation of *Arrhenius* temperature integral using a two-step linearly fitting process that proved to improve accuracy in non-isothermal kinetic data and based on that approximation, associated isoconversional equation is expressed as:

$$\ln\left(\frac{\beta}{T_\alpha^{1.894661}}\right) = \ln\left(\frac{AE_{a,\alpha}}{Rg(\alpha)}\right) + 3.635041 - 1.894661\ln\left(E_{a,\alpha}\right) - 1.001450\left(\frac{E_{a,\alpha}}{RT_\alpha}\right). \tag{13}$$

Plot of L.H.S. versus $(1/T_\alpha)$ of Eq. 13 should give straight line at constant α, whose slope is used to calculate the corresponding $E_{a,\alpha}$.

F–W–O method [13–16, 24–26]

It is also a widely employed integral isoconversional model-free method derived by using *Doyel's* approximation of $p(x)$ as:

$$\ln(p(x)) = -5.331 - 1.052x \quad (20 < x < 60). \tag{14}$$

Therefore, from Eqs. 5, 7, and 14 one can get the F–W–O expression:

$$\ln(\beta) = \ln\left(\frac{A * E_{a,\alpha}}{g(\alpha) * R}\right) - 5.331 - 1.052\left(\frac{E_{a,\alpha}}{RT}\right). \tag{15}$$

Thus, at constant α, plot of $\ln(\beta)$ versus $(1/T)$ should be straight line whose slope is used to evaluate corresponding $E_{a,\alpha}$.

Master plot analysis

Criado method [18–20, 32, 33]

The kinetic parameters (E_a, n, and A) of thermal degradation of present CNTs have been obtained by the non-isothermal analytical methods. The obeyed reaction mechanism(s) was determined using Criado method which can accurately determine mechanism of degradation process. First, Criado et al. defined a type of $Z(\alpha)$ function as:

$$Z(\alpha) = \frac{\left(\frac{d\alpha}{df}\right)}{\beta}\pi(x)T, \tag{16}$$

where $\pi(x)$ is an approximate expression obtained by integration against temperature and can be related with $p(x)$ as [33]:

$$\pi(x) = x\exp(x)p(x). \tag{17}$$

An approximate fourth rational expression of $p(x)$ proposed by Senum and Yang [35] and corrected by Flynn [36] can be expressed as:

$$p(x) = \frac{\exp(-x)}{x} * \left(\frac{x^3 + 18x^2 + 86x + 96}{x^4 + 20x^3 + 120x^2 + 240x + 120} \right) \quad (18)$$

for $x > 20$, Eq. 16 can give error less than $10^{-5}\%$, which is the basis for analyzing the TG data of present CNT specimens. Now, from Eqs. 2, 16, and 17 we get:

$$Z(\alpha) = f(\alpha)g(\alpha). \quad (19)$$

Combining Eq. 4 with 19, we should obtain:

$$Z(\alpha) = \frac{\beta}{A} g(\alpha) \frac{d\alpha}{dT} \exp\left(\frac{E_a}{RT}\right). \quad (20)$$

On the other hand, from Eqs. 2, 16, and 17 one may also get:

$$Z(\alpha) = \frac{d\alpha}{dT} x \exp(x) p(x) T = \frac{d\alpha}{dT} \frac{E_a}{R} \exp\left(\frac{E_a}{RT}\right) p(x). \quad (21)$$

In Eq. 21, the $d\alpha/dT$ values was obtained from corresponding DTG plots and Eq. 18 was used to evaluate the $p(x)$ expression where $x = E_a/RT$.

Finally, the master $Z(\alpha)$ versus α plots were evaluated according to Eq. 20 using commonly utilized $g(\alpha)$ expressions for describing different reaction mechanism [11, 12] and Eq. 21 was used to plot experimental $Z(\alpha)$ versus α curve according to TG data of specific CNT specimen. The mechanism(s) of thermal degradation of present CNT specimens were thus, easily and accurately predicted by comparing the master $Z(\alpha)$ versus α curves with the experimental $Z(\alpha)$ versus α curve.

Experimental

Raw materials

Supplier's specifications and nomenclature used in rest of the article of present SWNTs and MWNTs procured from two commercial agencies namely *Arry International GmbH*, *Germany* and *Shenzhen Nanotech Port Co.*, *China* are given in Table 1. Purity mentioned in Table 1 indicates weight percentage of particular CNT in 100 g batch.

TG analysis

Thermal oxidation experiments of present CNT samples were performed at three heating rates of 3, 6, and 10 K min^{-1} in *Netzsch STA-409* (*NETZSCH-Gerätebau GmbH*, *Germany*) TG instrument up to 1273 K in ambient air. In each experiment, 4–5 mg of CNT was taken in standard alumina crucible. Higher amount was not possible due to excessive fluffy structure of nanotubes. Based on the weight loss versus temperature data, first derivative i.e., differential thermogravimetric (DTG) plots were also obtained. TG data were finally treated with non-isothermal kinetic models to obtain the kinetic parameters of thermal oxidation. Changes in oxidation pattern (if any) of different CNTs obtained from TG, DTG plots, and kinetic parameters were correlated with their structural features.

Table 1 Specifications and nomenclature of CNT specimens

Parameters				
CNT type	SWNT	SWNT	MWNT	MWNT
Source	Arry	Shenzhen	Arry	Shenzhen
Symbol used	*SA*	*SS*	*MA*	*MS*
Purity/wt%	>90	>60	>95	>95
OD/nm	1–2	<2.0	>50	60–100
L/μm	5–20	5–15	<10	5–15
AC/wt%	<4.0	–	<3.0	3–5
Ash/wt%	<3.0	–	<1.0	<2.0
SSA/m^{-2} g^{-1}	>400	500–700	>120	40–70

OD outer diameter of CNT, *L* length of CNT, *AC* amorphous carbon, *SSA* special surface area

Electron microscopy

Fine scale morphology and nanostructure of all samples viz. *MA*, *MS*, *SA*, and *SS* were characterized by TEM using a *Tecnai* G^2*30ST* (*FEI Company*, *USA*) instrument. For TEM studies, small amount of CNT specimens were dispersed in isopropyl alcohol and sonicated for 15 min. TEM specimens were prepared by applying a drop of each suspension onto commercially available holey carbon coated copper (Cu) grids (*Ted Pella Inc.*, *USA*).

Results and discussion

Morphology of CNT specimens

From bright field TEM images of *MA* and *MS* specimens shown in Fig. 1a, b it appeared that *MA* had comparatively thinner tubes than *MS*. To quantify such observations, histograms of diameters of each MWNT were plotted on the basis of diameter measurement of 100 random CNTs within specimen tested. It can be easily visualized from Fig. 1c that while diameter of *MA* nanotubes was mostly within 20–60 nm, Fig. 1d indicates *MS* had nanotube diameter over a range of 20–100 nm. High resolution TEM (HRTEM) images of *MA* and *MS* specimens revealed that most of *MA* nanotubes had parallel graphene layers and clear internal channels (Fig. 2a) whereas, the presence of

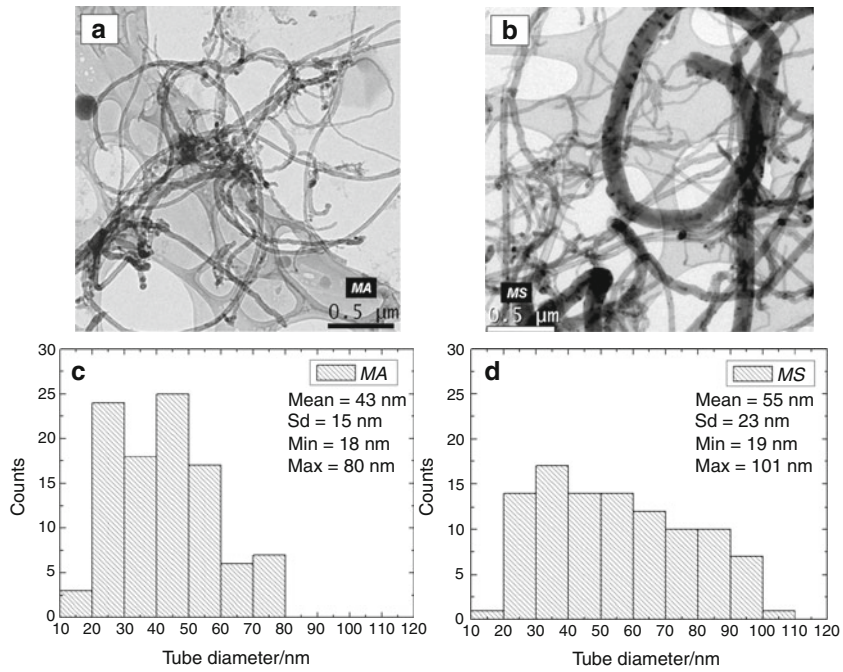

Fig. 1 Bright field TEM images of **a** *MA* (*scale bar* 0.5 μm) and **b** *MS* specimen (*scale bar* 0.5 μm); histograms of tube diameter of **c** *MA* and **d** *MS* specimen

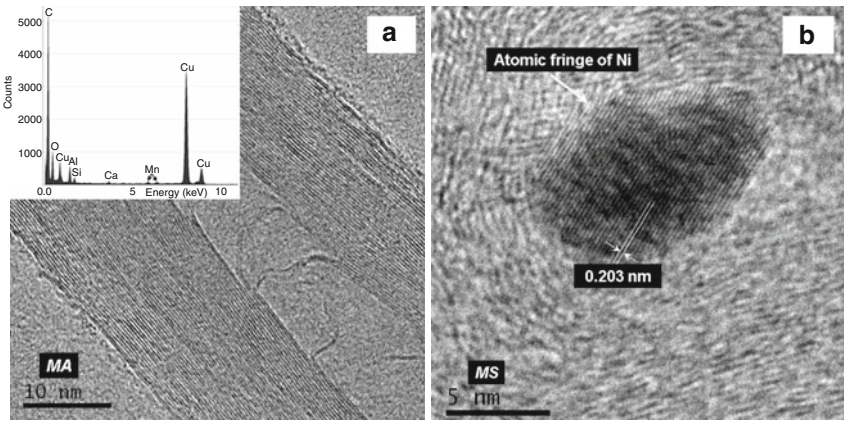

Fig. 2 HRTEM images of **a** *MA* (*scale bar* 10 nm); *inset* EDX of *MS* nanotubes and **b** *MS* (*scale bar* 5 nm) specimen showing graphene layer structure and impurity

nickel (Ni) nanoparticles was observed within the hollow cores (Fig. 2b) and at end-caps of *MS* nanotubes. The presence of Ni nanoparticles in as-received *MS* nanotubes has also been reported elsewhere [11]. For *MA* nanotubes, except carbon, different elemental peaks e.g., aluminum (Al), silicon (Si), oxygen (O), calcium (Ca), and manganese (Mn) were also detected (Fig. 2a, inset) indicating the presence of different types of impurities in *MA* than present in *MS*. Figures 3a, b shows TEM images of *SA* and *SS* nanotubes. The presence of cobalt (Co) nanoparticles as transition metal impurity in *SS* specimen was obtained during EDX analysis of TEM specimen (Fig. 3b, inset). Cu peaks appeared in the EDX patterns due to TEM grid used.

TG and DTG plots

From TG and DTG plots of *MA* and *MS* samples (Fig. 4a–d) it can be easily visualized that although both CNTs were primarily >95 wt% pure (Table 1), their degradation patterns in ambient were quite different mainly because of their structural dissimilarities as visualized during TEM studies and differences in impurity type/content and special surface area (SSA) (Table 1). Similar observations were made for SWNT specimens (Fig. 5a–d). The data obtained from TG and DTG plots of all four CNT specimens at each heating rate are given in Table 2 which indicates that the start (T_s) and end (T_e) temperatures of thermal degradation of *MA* and *MS* specimens were generally higher than those obtained for SWNTs (*SA* and *SS*) due to much thinner dimension and higher SSA of the latter (Table 1). However, Table 2 also indicates that although differences between T_s and T_e for *MA* and *SA* specimens were quite prominent, such differences were much lower for *MS* and *SS* specimens. As per Table 1, *SS* nanotubes contained 60 wt% SWNTs while *SA* was >90 wt% pure, thus, it might be possible that while oxidation of *SA* was primarily

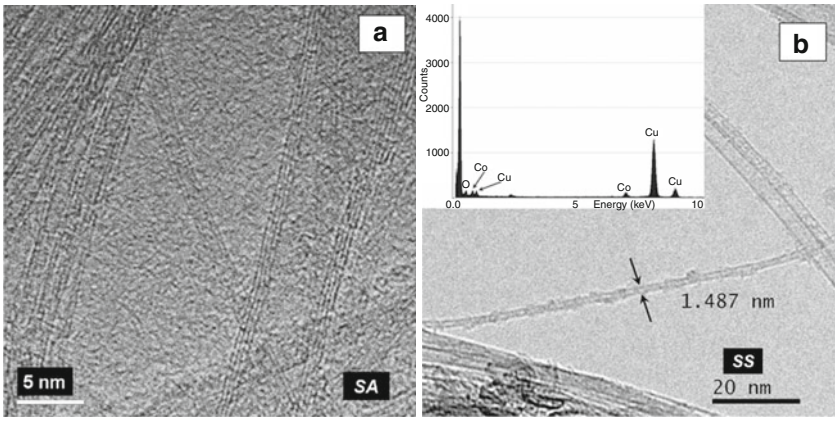

Fig. 3 HRTEM images of **a** *SA* (*scale bar* 5 nm) and **b** *SS* (*scale bar* 20 nm) specimen; *inset* EDX of *SS* specimen

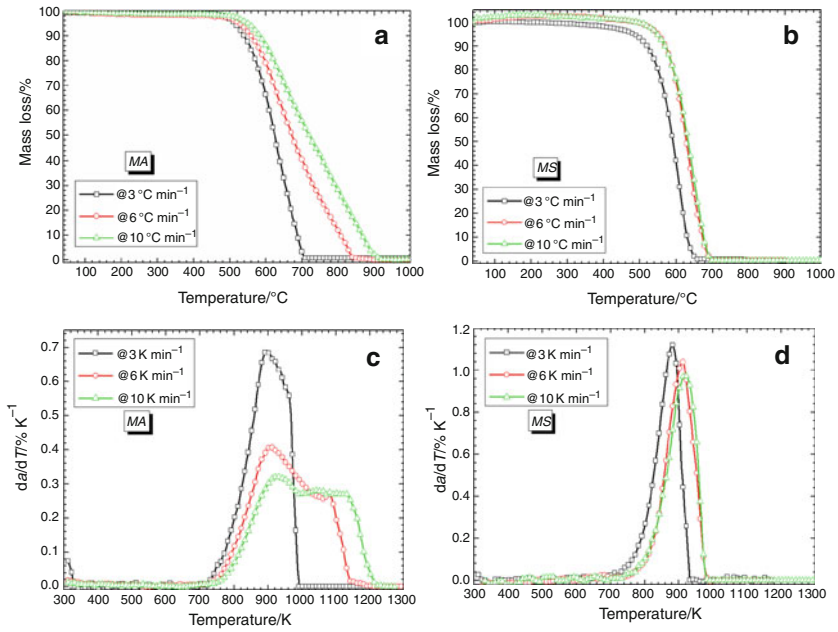

Fig. 4 TG plots of **a** *MA* and **b** *MS* specimen; DTG plots of **c** *MA* and **d** *MS* specimen

controlled by SWNTs, in *SS* both SWNT and other types of CNTs containing higher number of graphene layers per tube had equal contribution on degradation pattern that almost equalized the oxidation span of *MS* and *SS*. Further, the presence of transition metal nanoparticles i.e., Ni and Co in *MS* and *SS* as obtained during TEM analysis might also played a presiding role on overall degradation pattern of these nanotubes in ambient up to 1273 K.

Kinetic analysis

The *Arrhenius* parameters of thermal oxidation of present CNTs obtained from model-fitting CR method are given in Table 3 and matched well with literature data [7–11]. It may be seen from the table that for *MA* and *SA* specimens, reaction order was greatly influenced by experimental heating rate (Table 3). With increasing heating rate, reaction order increased significantly indicating delayed degradation of CNTs at faster heating rate possibly because of the fact that at faster heating rate, higher temperature was required to achieve the desired E_a for degradation to initiate. However, due to much thinner diameter and higher surface area of *SA* than that of *MA*, at each heating rate they oxidized relatively faster than *MA* leading to lower reaction order of the former (Table 3). Although, due to the same reason activation energy of *SA* specimen was fairly lower than that of *MA*, after initiation of reaction due to availability of significantly higher reaction sites in *MA* than *SA*, the pre-exponential factor of *MA* was found to be $\sim 10^3$ times higher than obtained for *SA* (Table 3). On contrary, such heating rate dependence of reaction order was not observed in *MS* and *SS* specimens. Regardless of heating rate used, they traced a first order reaction having slightly lower E_a and A values for *SS* than *MS* (Table 3). The

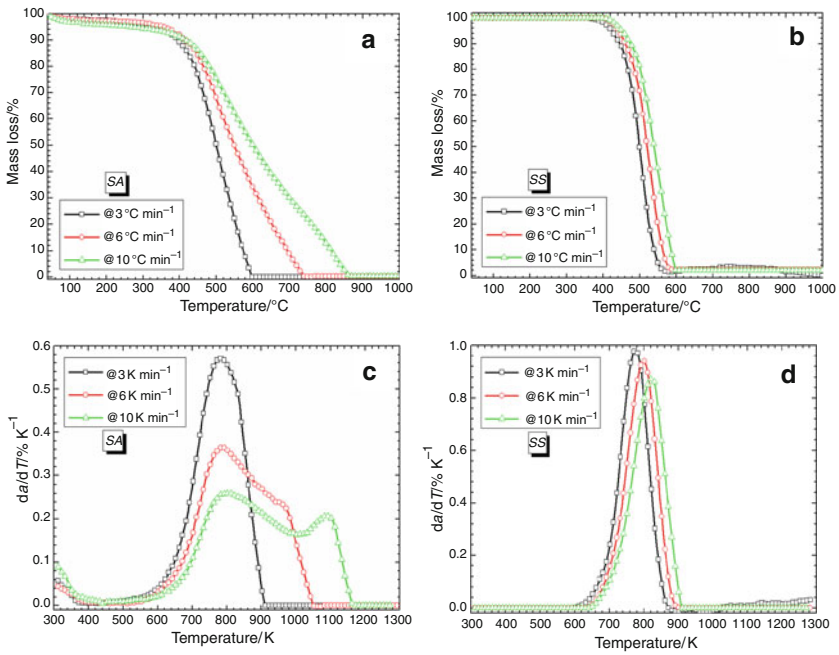

Fig. 5 TG plots of **a** *SA* and **b** *SS* specimen; DTG plots of **c** *SA* and **d** *SS* specimen

Table 2 Data obtained from TG and DTG plots of CNT specimens at three experimental heating rates

Sample	β	T_s	T_e	T_p	$(d\alpha/dT)_m$	$W\%$
MA						
	3	730	980	897	0.6883	50.02
	6	750	1110	907	0.4076	65.22
	10	760	1190	925	0.3209	69.90
MS						
	3	680	930	882	1.1256	31.09
	6	715	970	911	1.0419	38.93
	10	730	980	917	0.9853	39.14
SA						
	3	600	875	782	0.5720	44.59
	6	610	1015	787	0.3639	62.53
	10	620	1125	810	0.2555	66.37
SS						
	3	645	840	777	0.9655	43.87
	6	660	860	801	0.9397	41.29
	10	690	870	821	0.8706	41.79

β = experimental heating rate in °C min^{-1};T_p = temperature corresponded to maximum rate of decomposition in K; $(d\alpha/dT)_m$ = maximum rate of decomposition in % K^{-1}; $W\%$ = remaining weight of specimen at T_p in %

reason of getting mostly identical kinetic triplet for *MS* and *SS* specimens has been discussed in previous section.

Unlike CR method, the purpose of using multiple heating rate-based isoconversional techniques for kinetic studies of TG data of present CNT specimens was to check the extent of dependence of $E_{a,\alpha}$ on α. Change in $E_{a,\alpha}$ with increasing extent of conversion for *MA* and *SA* specimens are shown in Fig. 6a. It may be visualized from the figure that except isoconversional FR method, the other three methods were closely related. Such observation corroborates other reports and explanations behind this trend are also suggested [13, 24, 26, 28]. Figure 6a also indicates that local activation energy i.e., $E_{a,\alpha}$ of these two nanotube samples decreased sharply with increasing α possibly due to the fact that after splitting of initial C–C bond of graphene layer, formation of free reactive species became much easier that led to significant reduction in $E_{a,\alpha}$ as the reaction advanced. Further, increase in α at higher temperature might resulted in higher energy state of free carbon atoms formed from broken graphene layers that required lower kinetic energy ($E_{a,\alpha}$) of gaseous components of ambient air i.e., oxygen, carbon dioxide, and moisture (H_2O) to hit the active carbon atoms and produce reaction products [37]. While the maximum $E_{a,\alpha}$ obtained from *F–W–O* technique for *MA* and *SA* were $\sim$156 and $\sim$148 kJ mol^{-1}, respectively, at $\alpha \leq 0.1$, it reduced to only $\sim$54 and $\sim$36 kJ mol^{-1}, respectively, at $\alpha \approx 0.95$ (Fig. 6a). Thus, a decrease of $\sim$65 and $\sim$75% was observed for *MA* and *SA* specimens, respectively. Such gradual but strong decrease in local activation energy of nanotube oxidation obtained from isoconversional methods suggested that degradation kinetics of *MA* and *SA* specimens should follow complex reaction mechanism and can not be described by a single kinetic triplet obtained using model-fitting CR method. On contrary, such strong dependence of $E_{a,\alpha}$ with α was not observed for *MS* and *SS* specimens (Fig. 6b). More specifically, $E_{a,\alpha}$ remained

Table 3 Kinetic parameters of four CNT specimens obtained from CR method

Sample	β	E_α/kJ mol^{-1}	A/s^{-1}	n	R^2
MA					
	3	142.31	1.71×10^3	1.4	0 999
	6	152.65	8.99×10^3	3.3	0.999
	10	156.97	1.71×10^6	4.5	0.999
MS					
	3	164.16	7.37×10^6	1.0	0.999
	6	176.44	3.15×10^7	1.0	0 999
	10	178.19	5.81×10^7	1.0	0.999
SA					
	3	83.84	2.55×10^2	1.1	0.999
	6	94.29	2.13×10^3	2.9	0.999
	10	92.55	1.67×10^3	3.9	0.999
SS					
	3	140.58	2.23×10^6	1.0	0.998
	6	148.68	1.18×10^7	1.0	0.999
	10	148.56	1.12×10^7	1.0	0.999

β = experimental heating rate in °C min^{-1}

almost constant (Avg. $E_a \approx 150$ kJ mol^{-1}) within $0.25 \leq \alpha \leq 0.95$ for *MS* (Fig. 6b) where for *SS*, $E_{a,\alpha}$ varied within a low span of ~140 to ~184 kJ mol^{-1} (Fig. 6b). It might be possible that influence of transition metal catalyst nanoparticles e.g., Co, Ni present in as-received *MS* and *SS* nanotubes was significant on thermal oxidation of these two types of CNTs since it has been recently reported that the degradation trend in ambient air of metal catalyst-free *MS* after high temperature treatment in inert was quite different than that obtained in its as-received condition [11]. Further, higher $E_{a,\alpha}$ of *MS* than *MA* at each level of conversion might aroused due the lower SSA of former (Table 1) which required higher energy for degradation to continue.

For evaluating dependence of pre-exponential factor (A_α) on extent of conversion, the so-called artificial isokinetic relationship (IKR) was used which was although, initially proposed to investigate pre-exponential factor in isoconversional method as applied to single-step process, latter it was also used to isolate $\ln(A_\alpha)$ on α for a multi-step degradation [28, 29]. To perform this analysis, the following expression of *CR* method was utilized to get a set of E_a and A values using common $g(\alpha)$ expressions at a single heating rate [11, 12]:

$$\ln\left(\frac{g(\alpha)}{T^2}\right) = \ln\left(\frac{AR}{\beta E_a}\right) - \frac{E_a}{RT}. \quad (22)$$

Therefore, for a particular expression of $g(\alpha)$, plot of $\ln[g(\alpha)/T^2]$ versus $1/T$ should be a straight line whose slope and intercept allow an assessment of E_a and A, respectively.

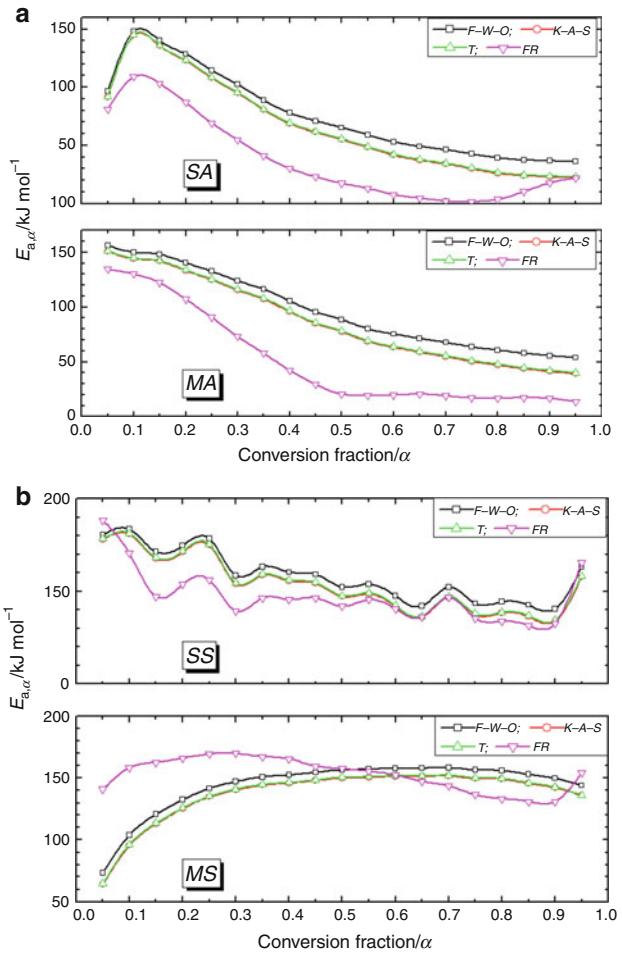

Fig. 6 Isoconversional plots of local activation energy ($E_{a,\alpha}$) of **a** *MA* and *SA* and **b** *MS* and *SS* specimens as a function of extent of conversion

The above procedure was performed for all other heating rates and other samples. Now, it was observed that at a particular heating rate and for a particular sample, E_a and A values at all $g(\alpha)$ follow a linear relation according to the following expression [28, 29]:

$$\ln A_i = m + nE_{a,i}, \quad (23)$$

where the subscript i in Eq. 23 refers to the ith $g(\alpha)$ model and $m = \ln(k_{iso})$ and $n = 1/RT_{iso}$. k_{iso} and T_{iso} are termed as *artificial isokinetic rate constant* and *artificial isokinetic temperature*, respectively. The *isokinetic* plot of all four CNT specimens at β of 10 °C min^{-1} is shown in Fig. 7 as an example. All plots showed acceptable linear fit having correlation coefficient (i.e., R) >0.97. Now, once the *isokinetic* parameters m and n were calculated for all samples, $E_{a,\alpha}$ values obtained from isoconversional analysis were incorporated in Eq. 23 to get corresponding $\ln(A_\alpha)$ values. The plots of $\ln(A_\alpha)$ versus α are shown in Fig. 8a, b. Clearly, dependence of pre-exponential factor on extent of

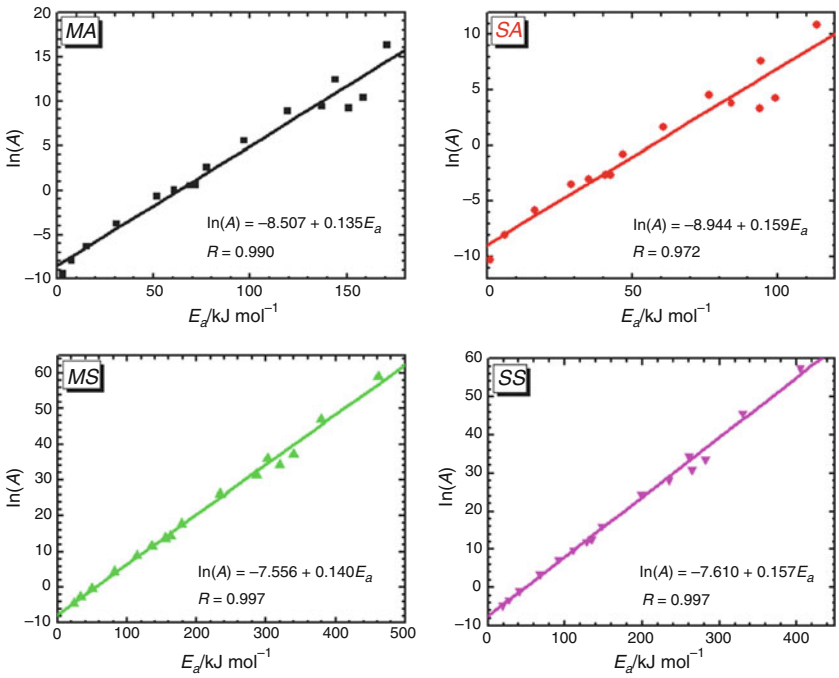

Fig. 7 Artificial IKR (ln(A) vs. E_a) using CR method for all CNT specimens at 10 °C min^{-1} heating rate

conversion was the same as observed for local activation energy. Further, Fig. 8a, b indicates that although decline in pre-exponential factor which is described as the tendency of a successful reaction to occur, was quite rapid for *MA* and *SA* specimens, ln(A_α) was maintained at a sufficiently higher level throughout the reaction span for *MS* and *SS* nanotubes. Thus, the complete degradation process of *MA* (Fig. 4a, c) and *SA* specimen (Fig. 5a, c) took longer time and lower (dα/dt) compared to *MS* (Fig. 4b, d) and *SS* nanotubes (Fig. 5b, d). Changes in $E_{a,\alpha}$ and A_α with extent of conversion of present as-received CNTs indicated that although they were primarily composed of carbon atoms, their diameter and length i.e., concentration of carbon atoms as well as type and concentration of impurities played an essential role on thermal degradation in ambient.

Criado method was used to find out involved reaction mechanism(s) in thermal oxidative degradation of present CNTs in ambient air. $Z(\alpha)$ versus α master curves were plotted according to Eq. 20 using common $g(\alpha)$ expressions [11, 12] and experimental $Z(\alpha)$ versus α plot was obtained according to Eq. 21. From Fig. 9a, b, it can be visualized that degradation reaction followed several mechanisms involving F_3, R_1, A_1F_1, and F_2 up to α (0.35 and 0.55 for *MA* and *SA* specimens, respectively). Comparison of experimental curves with master curves indicates that just during initiation of oxidation ($\alpha \approx 0.05$), the system was quite stable and thus, reaction initiated at a slower rate resulting in a third order reaction mechanism i.e., F_3 by gaining required E_a for degradation. However, with increasing temperature or degree of conversion (α from 0.10 to 0.20), supply of free carbon atoms from

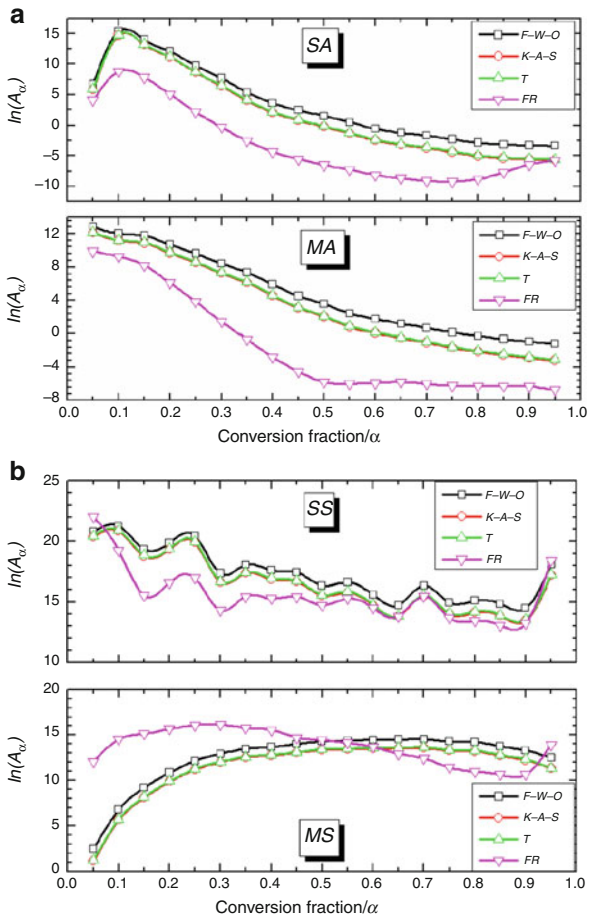

Fig. 8 Dependence of ln(A_α) on extent of conversion (α) evaluated from Eq. 23 for all four isoconversional methods of **a** *MA* and *SA* and **b** *MS* and *SS* specimens

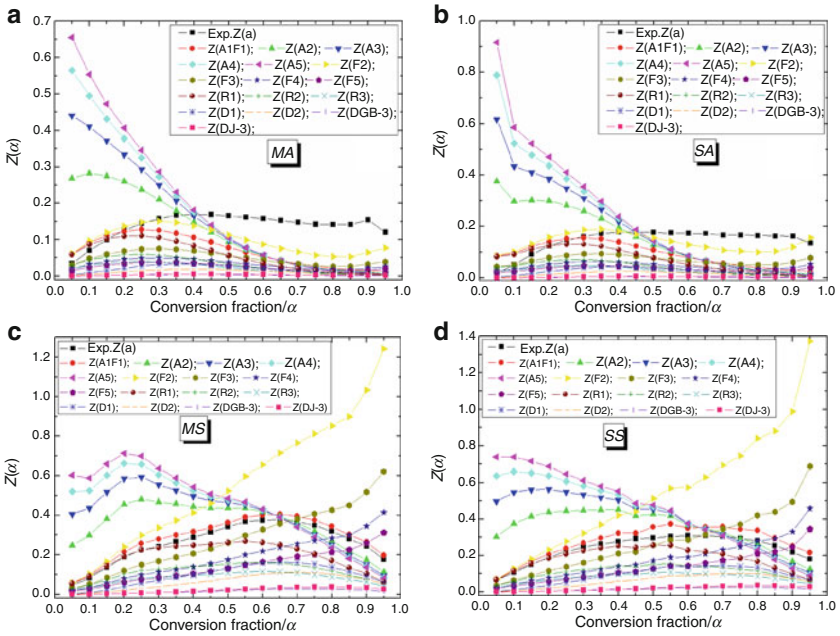

Fig. 9 Plots of $Z(\alpha)$ versus α comparing trend of experimental curve with those of master curves tracing different reaction mechanisms of **a** *MA*; **b** *SA*; **c** *MS*, and **d** *SS*. A_n: *Avrami-Erofeev* equations where $n = 1$–5; F_n: chemical reactions with $n = 1$–5; R_n = power law relations where $n = 1$–3, D_n: diffusion controlled reactions where $n = 1$–3 and subscripts GB and J stand for *Ginstling-Brounstein* and *Jander* equation, respectively

broken graphene layers increased significantly and therefore, the mechanism moved toward R_1 (i.e., zero order kinetics having much faster rate) followed by A_1F_1 mechanism (i.e., first order kinetics with reaction rate slower than R_1). Finally, at further higher conversion, supply of carbon atoms started to fall gradually resulting in slower degradation and thus, reaction path followed a second order reaction kinetics i.e., F_2 mechanism. As degradation moved toward end ($\alpha > 0.40$), experimental curve especially for *MA* specimen (Fig. 9a) sifted above F_2 and did not match well with any of the master curve suggesting that during this stage the system possibly followed a mechanism that was different than known reaction paths. On contrary, such complex reaction mechanism was not observed for *MS* and *SS* specimens (Fig. 9c, d). Up to $\sim 0.30\alpha$, oxidation of *MS* and *SS* specimens involved R_1 mechanism i.e., zero-order reaction kinetics indicating faster degradation of the specimens during $\alpha > 0.05$ to $\sim 0.30\alpha$ since during this stage the supply of free carbon atoms to produce reaction products was sufficient. Beyond 0.30α, degradation of *MS* and *SS* specimens traced a path passing through or very close to A_1F_1 master curve suggesting first order reaction at relatively slower rate than R_1 since formation of free carbon atoms decreased with increasing extent of conversion. However, unlike *MA* and *SA* specimens, *MS* and *SS* specimens did not pass through higher order reaction kinetics perhaps due to the fact that *MS* and *SS* specimens structurally possessed much better source of free carbon atoms due to the presence of higher number of graphene layers than *MA* or *SA* specimens.

Conclusions

Thermal degradation of SWNT or MWNT depend significantly on factors like geometry i.e., diameter and length of CNT used, surface area of particular CNT and impurity type and its concentration. For thinner CNTs having high SSA, E_a and A was quite less than those for thicker CNTs having lower SSA due to higher reactivity and less number of graphene layer involvements in oxidation process, respectively, of the former leading to lower reaction order values i.e., faster degradation. However, such trends might be overruled if impurity present in CNTs played key role in controlling the degradation. Similarly, depending on structural features, mechanism of thermal oxidation of CNTs might close to a single-step process or complex in nature involving several rate controlling reactions within the degradation span. Therefore, for this system i.e., CNT to get truthful kinetic data i.e., to assess the real dependence of activation energy on temperature and/or degree of conversion, model-free methods should always be preferred instead of model-fitting techniques.

Acknowledgements The authors express their sincere gratitude to the Director, Central Glass and Ceramic Research Institute (CG & CRI), India for his kind permission to publish this study. The authors are also grateful to the members of Analytical Facility Division and Materials Characterization Unit of CG & CRI, India for their extensive help in carrying out all the TEM analysis and TG experiments, respectively. The first author acknowledges the financial support of the Council of Scientific and Industrial Research (CSIR), India.

References

1. Terrones M. Science and technology of the twenty-first century: synthesis, properties, and applications of carbon nanotubes. Annu Rev Mater Res. 2003;33:419–501.
2. Breuer O, Sundararaj U. Big returns from small fibers: a review of polymer/carbon nanotube composites. Polym Compos. 2004; 25:630–41.
3. Samal SS, Bal S. Carbon nanotube reinforced ceramic matrix composites—a review. J Miner Mater Character Eng. 2008;7(4): 355–70.
4. Bakshi SR, Lahiri D, Agarwal A. Carbon nanotube reinforced metal matrix composites–a review. Int Mater Rev. 2010;55(1): 41–64.
5. Song W-l, Cao M-S, Hou Z-l, Yuan J, Fang X-Y. High-temperature microwave absorption and evolutionary behavior of multi-walled carbon nanotube nanocomposite. Scr Mater. 2009;61: 201–4.
6. Chen Z-K, Yang J-P, Ni Q-Q, Fu S-Y, Huang Y-G. Reinforcement of epoxy resins with multi-walled carbon nanotubes for enhancing cryogenic mechanical properties. Polymer. 2009;50: 4753–9.
7. Illeková E, Csomorová K. Kinetics of oxidation in various forms of carbon. J Therm Anal Calorim. 2005;80:103–8.
8. Brukh R, Mitra S. Kinetics of carbon nanotube oxidation. J Mater Chem. 2007;17:619–23.
9. Vignes A, Dufaud O, Perrin L, Thomas D, Bouillard J, Janès A, et al. Thermal ignition and self-heating of carbon nanotubes: from thermokinetic study to process safety. Chem Eng Sci. 2009;64: 4210–21.
10. Sarkar S, Das PK, Bysakh S, Dasgupta K. Evaluation of thermal stability of commercial multiwalled carbon nanotubes. First Asian Carbon Conference, New Delhi, 2009.
11. Sarkar S, Das PK, Bysakh S. Effect of heat treatment on morphology and thermal decomposition kinetics of multiwalled carbon nanotubes. Mater Chem Phys. 2011;125:161–7.
12. Al-Othman AA, Al-Farhan KA, Mahfouz RM. Kinetic analysis of nonisothermal decomposition of ($Mg_5(CO_3)_4(OH)_2{\cdot}4H_2O/5Cr_2O_3$) crystalline mixture. J King Saud Univ (Sci). 2009;21:133–43.
13. Janković B, Mentus S, Jelic D. A kinetic study of non-isothermal decomposition process of anhydrous nickel nitrate under air atmosphere. Physica B. 2009;404:2263–9.
14. Boonchom B, Danvirutai C, Thongkam M. Non-isothermal decomposition kinetics of synthetic serrabrancaite ($MnPO_4{\cdot}H_2O$) precursor in N_2 atmosphere. J Therm Anal Calorim. 2010;99: 357–62.
15. Boonchom B. Kinetic and thermodynamic studies of $MgHPO_4{\cdot}3H_2O$ by non-isothermal decomposition data. J Therm Anal Calorim. 2009;98:863–71.
16. Jiao-qiang Z, Hong-xu G, Li-hong S, Rong-zu H, Feng-qi Z, Bozhou W. Non-isothermal thermal decomposition reaction kinetics of 2-nitroimino-5-nitro-hexahydro-1,3,5-triazine (NNHT). J Hazard Mater. 2009;167:205–8.
17. Wang Y-F, Liu J-F, Xian H-D, Zhao G-L. Synthesis, crystal structure, and kinetics of the thermal decomposition of the nickel(ii) complex of the Schiff base 2-[(4-Methylphenylimino)methyl]-6-methoxyphenol. Molecules. 2009;14:2582–93.
18. Chen Y, Wang Q. Thermal oxidative degradation kinetics of flame-retarded polypropylene with intumescent flame-retardant master batches in situ prepared in twin-screw extruder. Polym Degrad Stabil. 2007;92:280–91.
19. Doğan F, Kaya I, Bilici A. Non-isothermal degradation kinetics of poly (2,2′-dihydroxybiphenyl). Polym Bull. 2009;63:267–82.
20. Doğan F, Kaya I, Bilici A, Saçak M. Thermal decomposition kinetics of azomethine oligomer and its some metal complexes. J Appl Polym Sci. 2010;118:547–56.
21. Brown ME, Maciejewski M, Vyazovkin S, Nomen R, Sempere J, Burnham A, et al. Computational aspects of kinetic analysis Part A: the ICTAC kinetics project-data. Thermochim Acta. 2000;355: 125–43.
22. Vyazovkin S. Computational aspects of kinetic analysis. Part C. The ICTAC kinetics project-the light at the end of the tunnel? Thermochim Acta. 2000;355:155–63.
23. Vyazovkin S. Reply to "What is meant by the term 'variable activation energy' when applied in the kinetics analyses of solid state decompositions (crystolysis reactions)?" Thermochim Acta. 2003;397:269–71.
24. Pratap A, Rao TLS, Lad KN, Dhurandhar HD. Isoconversional vs. model fitting methods: a case study of crystallization kinetics of a Fe-based metallic glass. J Therm Anal Calorim. 2007;89: 399–405.
25. Burnham AK, Dinh LN. A comparison of isoconversional and model-fitting approaches to kinetic parameter estimation and application predictions. J Therm Anal Calorim. 2007;89:479–90.
26. Janković B. Kinetic analysis of the nonisothermal decomposition of potassium metabisulfite using the model-fitting and isoconversional (model-free) methods. Chem Eng J. 2008;139:128–35.
27. Galwey AK. What is meant by the term 'variable activation energy' when applied in the kinetic analyses of solid state decompositions (crystolysis reactions)? Thermochim Acta. 2003;397:249–68.
28. Janković B, Adnađević B, Jovanović J. Application of model-fitting and model-free kinetics to the study of non-isothermal dehydration of equilibrium swollen poly (acrylic acid) hydrogel: thermogravimetric analysis, Thermochim Acta. 2007;452:106–15.
29. Pourghahramani P, Forssberg E. Reduction kinetics of mechanically activated hematite concentrate with hydrogen gas using nonisothermal methods. Thermochim Acta. 2007;454:69–77.
30. Serra R, Nomen R, Sempere J. The non-parametric kinetics: a new method for the kinetic study of thermoanalytical data. J Therm Anal Calorim. 1998;52:933–43.
31. Serra R, Nomen R, Sempere J. A new method for the kinetic study of thermoanalytical data: the non-parametric kinetics method. Thermochim Acta. 1998;316:37–45.
32. Criado JM, Málek J, Ortega A. Applicability of the master plots in kinetic analysis of a non-isothermal rate. Thermochim Acta. 1989;147:377–85.
33. Tiptipakorn S, Damrongsakkul S, Ando S, Hemvichian K, Rimdusit S. Thermal degradation behaviors of polybenzoxazine and silicon-containing polyimide blends. Polym Degrad Stabil. 2007; 92:1265–78.
34. Tang W, Liu Y, Zhang H, Wang C. New approximate formula for Arrhenius temperature integral. Thermochim Acta. 2003;408: 39–43.
35. Senum GI, Yang RT. Rational approximations of the integral of the Arrhenius function. J Therm Anal Calorim. 1977;11:445–9.
36. Flynn JH. The 'temperature integral': its use and abuse. Thermochim Acta. 1997;300:83–92.
37. Tesner PA. The activation energy of gas reactions with solid carbon. Eight International Symposium on Combustion, Williams & Wilkins Co., Baltimore, USA, 1962, pp. 807–13; Discussion by Essenhigh RH. pp. 813–14.